Journal of Materials Chemistry B

PAPER

View Article Online
View Journal | View Issue

Cite this: J. Mater. Chem. B, 2019, 7, 6855

Molecular isomerization triggered by H_2S to an NIR accessible first direct visualization of Ca^{2+}-dependent production in living HeLa cells†

Ying Wen,[a] Fangjun Huo,[b] Junping Wang[a] and Caixia Yin *[a]

Received 2nd September 2019,
Accepted 29th September 2019

DOI: 10.1039/c9tb01885a

rsc.li/materials-b

Few studies determined the role of intracellular labile Ca^{2+} in H_2S homeostasis. Undoubtedly, fluorescent probes are powerful tools for exploring the question because of their unique advantages: non-destruction, visualization, and multi-levels imaging. Herein, a near-infrared (λ_{em} = 687 nm) and methylene blue chromophore-based fluorescent probe (**MB1**) for H_2S was rationally developed. Based on its high sensitivity and selectivity, **MB1** was employed to image the concentration change of H_2S, upon stimulating it with ionomycin (a specific calcium ionophore). We found that the intracellular labile Ca^{2+} acted as a promotor for H_2S production in living cells. Furthermore, cystathionine γ-lyase (CSE) might have functioned as a positive mediator of Ca^{2+}-dependent H_2S production. These direct and visible links for H_2S/Ca^{2+} will help us to understand the complex signaling in a better way.

Introduction

Hydrogen sulfide (H_2S), the third gasotransmitter,[1,2] is produced enzymatically by cystathionine γ-lyase (CSE), cystathionine β-synthase (CBS), or the cooperative effect of cysteine aminotransferase (CAT) and 3-mercaptopyruvate sulfurtransferase (3-MST).[3] Alternate pathways for the formation of H_2S is nonenzymatic pathways, such as changing from persulfide at the expense of reductants. H_2S can regulate the insulin release,[4] induce angiogenesis,[5] and protect neurons from the oxidative stress,[6] which has been reported to associate with diseases, such as liver cirrhosis,[7] Alzheimer's disease,[8] diabetes,[9] Down syndrome,[10] and hypertension.[11]

Calcium ion (Ca^{2+}), as a second messenger, was involved in a broad spectrum of intracellular signal transduction. Although H_2S or Ca^{2+} signal transduction pathways have been characterized, few studies examined the relationship between H_2S and Ca^{2+} levels in living cells. As reported, the specific enzymes involved in the H_2S production, such as CAT[12,13] and CSE,[14,15] were regulated by the intracellular calcium/calmodulin. However, a similar observation can not be obtained by other laboratories.[1] Thus, the role of intracellular labile Ca^{2+} in the H_2S hemostasis is considered ambiguous.

There is no denying that direct observation and image analysis is one of the most persuasive evidences to solve this problem.[16–27] Thus, the development of fluorescent probes is of utmost importance. In this process, the selection of a fluorophore and the design of a reaction site need to cater to the probe's practical applications. Herein, *via* a smart design, the molecular isomerization and self-immolative triggered by H_2S was employed in a near-infrared region (λ_{em} = 687 nm) methylene blue dye with excellent biocompatibility and optical performance,[28,29] to construct an H_2S probe (denominated in **MB1**) with enhanced sensitivity and selectivity. The presence of high concentrations of calcium ions did not interfere with the turn-on response of **MB1** for H_2S. Therefore, **MB1** was used to detect the levels of H_2S upon incubating the cells with ionomycin (a specific calcium ionophore). The cell imaging experiments clearly suggested that the levels of H_2S increased sharply as the concentration of Ca^{2+} concentration increased. Namely, the intracellular labile Ca^{2+} acted as a promotor of H_2S production. Furthermore, with the assistance of **MB1**, it was found that CSE might have played an important 'mediator' role. Thus, this data will help us to understand the complex pathway interactions between Ca^{2+} and H_2S in living cells in a better way.

Experimental section

Materials

All the starting materials were obtained from commercial suppliers. *S*-Nitroso-*N*-acetyl-DL-penicillamine (SNP) was purchased from Sigma-Aldrich (St Louis, MO, USA). 4-Amino benzene methanol was purchased from Alfa Aesar (Ward Hill, MA, USA). Ionomycin, 4-(6-acetoxymethoxy-2,7-dichloro-3-oxo-9-xanthenyl)-4′-methyl-2,2′(ethylenedioxy)dianiline-*N*,*N*,*N*′,*N*′-tetraacetic acid

[a] Key Laboratory of Chemical Biology and Molecular Engineering of Ministry of Education, Key Laboratory of Materials for Energy Conversion and Storage of Shanxi Province, Institute of Molecular Science, Shanxi University, Taiyuan 030006, China. E-mail: yincx@sxu.edu.cn

[b] Research Institute of Applied Chemistry, Shanxi University, Taiyuan 030006, China

† Electronic supplementary information (ESI) available: The details of characterization of compounds and additional data. See DOI: 10.1039/c9tb01885a

tetrakis(acetoxymethyl) ester (**Fluo-3AM**), CCK-8, and cell culture reagents were purchased from Beyotime Co., Ltd (Shanghai, China).

Instruments

^{1}H NMR (600 MHz) spectra and the high-resolution mass spectra (HR-MS) were recorded on a Bruker Avance III HD spectrometer and AB Sciex Triple TOF 5600 instrument, respectively. The UV-visible spectra and steady-state emission experiments were recorded on a Hitachi U-3900 spectrometer and a Hitachi F-7000 spectrometer, respectively. The cell imaging experiments were performed using a Zeiss LSM880 Airyscan laser confocal scanning microscope. The *in vivo* imaging assays were performed on the Bruker In-Vivo FX Pro small animal optical imaging system.

Synthesis details of MB1

The synthesis route of **MB1** is shown in Scheme S1 in the ESI.†

C1. C1 was synthesized as per the previously reported method.[30]

FDOCl-2. FDOCl-2 was the gift of Professor Tao Yi and Dr Peng Wei (Department of Chemistry, Fudan University, Shanghai, China).[25]

MB1. C1 (70 mg, 0.47 mmol), **FDOCl-2** (140.1 mg, 0.40 mmol), Na_2CO_3 (124.4 mg, 1.17 mmol), and DMAP (50.7 mg, 0.4 mmol) were dissolved in 20 mL anhydrous DCM. The reaction mixture was cooled to 0 °C and stirred overnight under nitrogen. The reaction was monitored by TLC. The product was purified *via* column chromatography using ethyl acetate/petroleum ether (1/4, v/v) as an eluent to obtain **MB1** as a white powder. Yield 40%; ^{1}H NMR (600 MHz, $CDCl_3$) δ 7.33 (d, J = 7.7 Hz, 4H), 7.00 (d, J = 7.8 Hz, 2H), 6.66 (s, 2H), 6.60 (d, J = 7.8 Hz, 2H), 5.18 (s, 3H), 2.93 (s, 12H). ^{13}C NMR (151 MHz, DMSO) δ 153.52 (s), 139.06 (s), 133.26 (s), 131.97 (s), 129.49 (s), 127.48 (s), 126.97 (s), 119.15 (s), 110.86 (s), 109.72 (s), 66.55 (s), 48.60 (s). HR-MS: for $C_{24}H_{24}N_6O_2SNa^+$ $[M + Na]^+$ calc. 483.1579, found 483.1573.

Fluorescence quantum yield determination

The fluorescence quantum yield (Φ_F) was estimated by a comparative method, where unsubstituted Zn(II) phthalocyanine (ZnPc) was used as the ref. 31 The reference value of Φ_F was found to be 0.18 in DMSO for ZnPc.[32] The fluorescence quantum yield was calculated using: $\Phi_F = \Phi_F(\mathrm{Std}) \times (A_{\mathrm{Std}}/A) \times (F/F_{\mathrm{Std}}) \times (n^2/n_{\mathrm{Std}}{}^2)$, where the subscripts Std refer to the standard sample. F and F_{Std} are the areas under the fluorescence emission curves of the sample and the standard, respectively. A and A_{Std} are the respective absorbances of the sample and standard at the excitation wavelengths. The n and n_{Std} are the refractive indices of the solvents used for the sample and standard, respectively.[33] The absorbance of the solutions at the excitation wavelength ranged between 0.1 to 0.02.

Cell culture and confocal laser scanning microscope (CLSM) imaging

The HeLa cells were cultured in RPMI 1640 media supplemented with the 10% fetal bovine serum at 37 °C in a humidified atmosphere containing 5% CO_2. The cells were plated on 14 mm glass coverslips overnight, washed with PBS, and then incubated with **MB1** (5 μM, 30 min) and/or **Fluo-3 AM** (1 μM, 20 min) at 25 °C. After washing three times, the cells were subjected to CLSM imaging. The red channel (690 ± 30 nm) was used to collect the **MB1** signal under 633 nm as the excitation wavelength. In the detection experiments of exogenous and endogenous H_2S, the **MB1**-loaded HeLa cells were pre-incubated with SNP (100 μM, 30 min) or Na_2S (160 μM, 30 min). In the Ca^{2+}-triggered experiments, the **MB1**-loaded or **Fluo-3 AM**-loaded HeLa cells were pre-incubated with 200 μM $CaCl_2$ or 1 μM ionomycin for 1.5 h. The green channel was set at 525 ± 25 nm (λ_{ex} = 488 nm) for **Fluo-3AM**.

In vivo fluorescence images of BALB/c nude mice

BALB/c-nude mice were purchased from Sparford Biotechnology Co., Ltd (Beijing, China). All the animal experiments were performed by following the protocols approved by the Radiation Protection Institute of Drug Safety Evaluation Center in China (Production license: SYXK (Jin) 2018-0005). 50 μL of **MB1** (1 mM) and 50 μL of Na_2S (1 mM) were injected into the right tibiotarsal joints (right ankles) of 6–8 week-old BALB/c Nude Mice. The imaging assays were performed in a small animal optical imaging system, with an excitation filter of 630 nm and an emission filter of 700 nm.

Results and discussion

Synthesis of MB1

For constructing specifically the H_2S-responsive probe, we selected methylene blue as a fluorescent chromophore. A previously reported reaction strategy of H_2S and aryl azides to amines was adopted.[34,35] The 4-azidobenzyl group, as a self-immolative aryl azide linker, was chosen to link to methylene blue. First, we synthesized 4-azido benzene methanol from 4-amino benzene methanol and NaN_3. Then, the condensation reaction between 4-azido benzene methanol and the carbamoyl chloride derivative of methylene blue (**FDOCl-2**) was employed to obtain **MB1**. The details of the characterization of **MB1** are shown in Fig. S1–S3 of the ESI.†

Capability of MB1 to detect H_2S in the solution

To guide the follow-up cell experiments, we first examined the spectral properties of **MB1** in Fig. 1. 5 μM of **MB1** (DMSO : PBS, 1 : 1, v/v) did not show any obvious absorption and fluorescent emission peak. However, after adding H_2S (donors: 160 μM Na_2S), **MB1** displayed one major absorption band in the wavelength range of 550 nm to 700 nm (centered at 666 nm, ε = 20 600 M^{-1} cm^{-1}, Fig. 1A), which was observed to increase with time, thereby suggesting that the chemical structure of **MB1** has changed. Moreover, the high-resolution mass spectra analysis (Fig. S4, ESI†) confirmed that the new product was methylene blue, which was recovered *via* the self-immolative release from **MB1** and molecular isomerization after reduction by H_2S (Scheme 1).

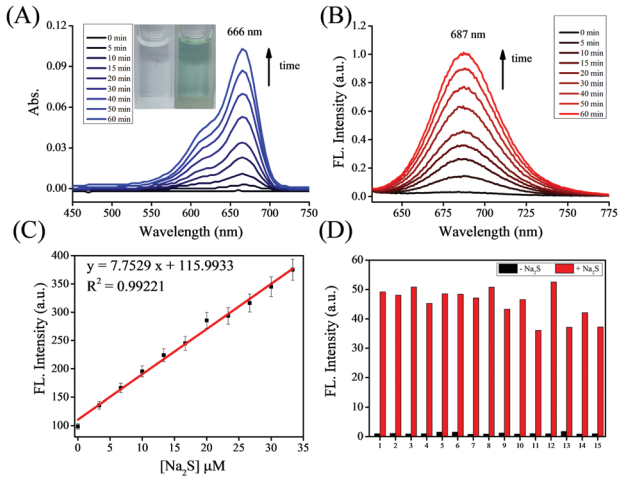

Fig. 1 The changes in the absorption (A) and fluorescence (B) spectra of **MB1** (5 μM, DMSO : PBS, 1 : 1, v/v) over time after addition of Na_2S (160 μM). Insets of (A): the color changes of **MB1** in the absence and presence of H_2S. (C) Plot of fluorescence intensity at 687 nm (F_{687}) for **MB1** (5 μM) *vs.* [Na_2S] from 1 to 35 μM. Each data was collected after 1 h upon the addition of Na_2S. The error bars and average values are shown for experiments repeated 3 times independently. (D) F_{687} of **MB1** (5 μM) in response to various other biologically relevant species after 1 h at 25 °C. Black bar of 1 was blank; 2 to 15 represent 500 μM SO_4^{2-}, $S_2O_3^{2-}$, SCN^-, Ca^{2+}, Mg^{2+}, K^+, Na^+, GSH, L-Me, L-Cys, L-Ala, L-Hcy, H_2O_2, and HClO, respectively. Red columns represent the extra addition of 160 μM Na_2S. λ_{ex} = 600 nm.

In addition, **MB1** showed a fluorescence turn-on response toward H_2S. Upon treatment of 5 μM of **MB1** with H_2S, a near-infrared fluorescence emission ranging from 632 nm to 775 nm (majored in 687 nm, Fig. 1B) was observed, which drastically increased over time, with 600 nm excitation. After reacting with H_2S, the fluorescence quantum yield (Φ_F) of **MB1** increased from less than 0.02 to 0.13. The same fluorescence spectral experiments were performed without H_2S (Fig. S5, ESI†), and it was observed that the absorption and fluorescence spectra did not show any change, which in turn indicated the stability of **MB1**. The dynamic curve of **MB1** is shown in Fig. S6 (ESI†).

The concentration of Na_2S varying from 1 to 35 μM showed a better linear relationship (R^2 = 0.9931) with the fluorescence intensities at 687 nm (F_{687}, Fig. 1C). The detection limit was calculated to be 0.32 μM by using the formula of $3\sigma/k$, where k is the slope in Fig. 1C, and σ is the standard deviation of the blank samples.

Importantly, **MB1** exhibited high chemoselectivity in the spectroscopic response. When treated with various biomolecules, including metal ions (Ca^{2+}, Mg^{2+}, K^+, and Na^+), amino acid (L-Cys, L-Ala, and L-Hcy), reactive sulfur species ($S_2O_3^{2-}$, SO_4^{2-}, and SCN^-), GSH, H_2O_2, and HClO, F_{687} of the probe exhibited no changes, compared with a 49.2-fold increase upon the stimulation of Na_2S (Fig. 1D). Even in the presence of the interfering species, particularly Ca^{2+}, **MB1** still showed an excellent response to H_2S. Thus, these results demonstrated that **MB1** was a highly sensitive and selective probe towards H_2S.

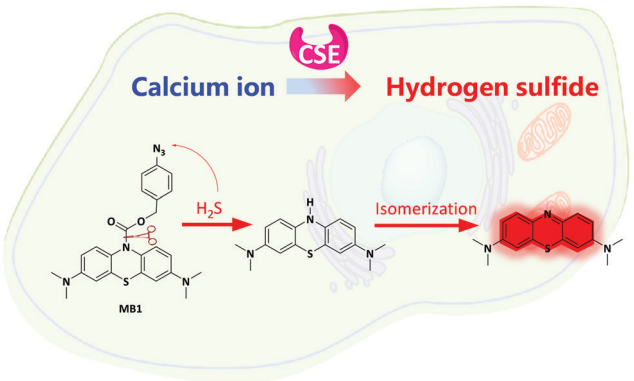

Scheme 1 The chemical structure, response mechanism, and potential imaging applications of **MB1**.

Detection of H_2S with MB1 in living cells

Prior to the imaging application in living cells, the CCK-8 assay was performed to verify the low acute toxicity of **MB1** to living HeLa cells. The viabilities were found to be >96% at 5 h or 10 h when 1–10 μM of **MB1** was incubated (Fig. S7, ESI†), thereby clearly suggesting that **MB1** possessed excellent biocompatibility.

We next assessed whether the probe had sufficient sensitivity to visualize the exogenous and endogenous H_2S in HeLa cells using a confocal laser scanning microscope (CLSM). The **MB1**-loaded (5 μM, 25 °C, 30 min) HeLa cells were imaged from the red fluorescence channel (690 ± 30 nm). Upon pre-incubation with 160 μM of Na_2S for 30 min, the HeLa cells (Fig. 2a7) showed strong red fluorescence, clearly indicating the good cell-membrane permeability and H_2S response ability of **MB1** in living cells. Then, to verify the high sensitivity of the probe, **MB1** was employed to monitor the H_2S generated endogenously in living cells (Fig. 2a4). Moreover, SNP (a commercial NO donor) was used to stimulate the generation of endogenous H_2S.[36] The increased fluorescence signal was observed in **MB1**-treated HeLa cells pre-incubated with 100 μM of SNP for 30 min. These results indicated that **MB1** was capable of visualizing endogenous H_2S generation. **MB1** can also be used to correlate different levels of H_2S *in vivo* with the intensity being in the NIR emissions range (Fig. S8, ESI†).

After verifying the high selectivity and sensitivity, **MB1** was used to directly evaluate the change in the H_2S level of the Ca^{2+}-treated cells. Compared with the only probe group (**MB1**, 5 μM, 30 min, Fig. 3b1), the red fluorescence signal (690 ± 30 nm) in the HeLa cells of Ca^{2+}-pretreated (200 μM, 1.5 h) group (Fig. 3c1) markedly increased. In addition, the corresponding average fluorescence intensities of the cells shown in Fig. 3b1 and c1 presented statistical changes of $p < 0.05$. However, upon co-incubating the cells with 200 μM of EDTA (metal ion chelating agent), the red fluorescence intensity of the cells stimulated by Ca^{2+} (Fig. 3e1, $p < 0.05$) was reduced significantly. Further, taking into consideration that Ca^{2+} homeostasis is tightly controlled in living cells, a universal Ca^{2+} fluorescent probe (**Fluo-3 AM**) was employed to demonstrate that incubation with 200 μM $CaCl_2$ can induce a slight increase in the intracellular labile Ca^{2+} concentrations (Fig. 3c3). The fluorescence signal of **Fluo-3 AM** was collected within the green channel (525 ± 25 nm), under 488 nm as an excitation

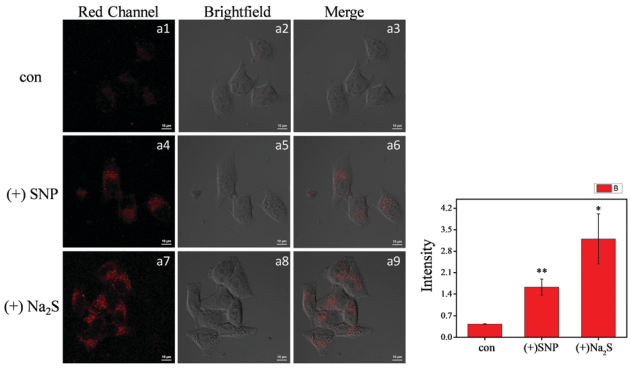

Fig. 2 (left) The CLSM images of HeLa cells loaded with 5 μM of **MB1**. The cells were pre-incubated with SNP (100 μM, 30 min) or Na_2S (160 μM, 30 min); red channel, 690 ± 30 nm; λ_{ex} = 633 nm; scale bar = 10 μm. (right) Corresponding average fluorescence intensities of the respective cells in the left images. Statistical analyses were employed with the Student's *t*-test (n = 3). Compared with the control group: $^{*}p < 0.05$, $^{**}p < 0.01$, and error bars are ±S.D.

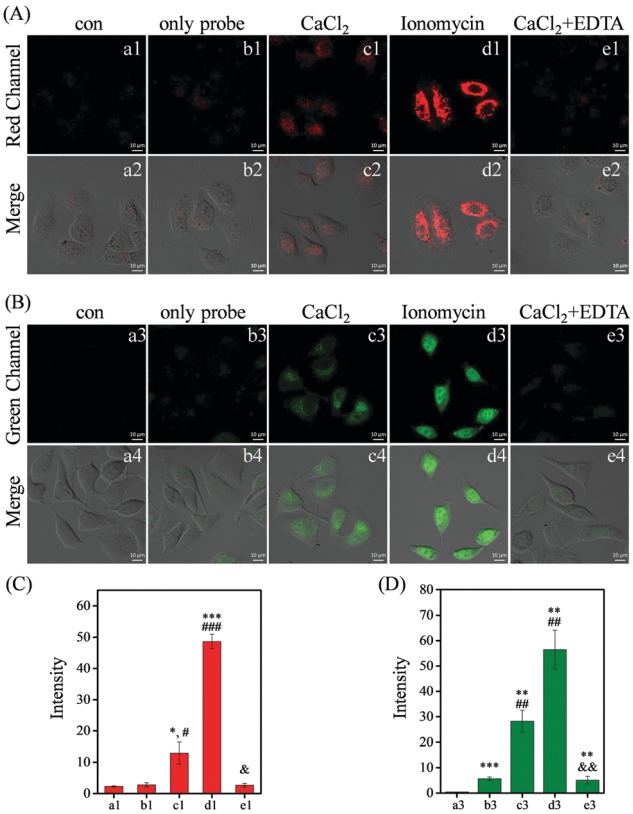

Fig. 3 The CLSM images of (A) **MB1** (5 μM, 30 min) or (B) **Fluo-3 AM** (1 μM, 20 min)-loaded HeLa cells. (a1–a4) control group; before being loaded with **MB1** or **Fluo-3 AM**, the HeLa cells were pre-incubated with (b1–b4) only PBS; (c1–c4) $CaCl_2$; (d1–d4) ionomycin; (e1–e4) $CaCl_2$ and EDTA at 37 °C for 90 min. $CaCl_2$: 200 μM; ionomycin: 1 μM; EDTA: 200 μM; Red channel, 690 ± 30 nm, λ_{ex} = 633 nm for **MB1**; Green channel, 525 ± 25 nm, λ_{ex} = 488 nm for **Fluo-3 AM**; Scale bar = 10 μm. (C) or (D) Corresponding average fluorescence intensities of cells in (A) or (B), respectively. Statistical analyses were employed with Student's *t*-test (n = 3). Compared with the control (a1 or a3) group: $^{*}p < 0.05$, $^{**}p < 0.01$, and $^{***}p < 0.001$. Compared with the group (b1 or b3) having only probe: $^{\#}p < 0.05$, $^{\#\#}p < 0.01$, and $^{\#\#\#}p < 0.001$. Compared with the $CaCl_2$-treated (c1 or c3) group; $^{\&}p < 0.05$, $^{\&\&}p < 0.01$, and error bars are ±S.D.

wavelength. Therefore, these data indicated that in HeLa cells, the stimulation of Ca^{2+} could induce the H_2S explosion.

Ionomycin was employed to further verify the above result, which is known to raise the intracellular level of Ca^{2+} *via* allowing direct Ca^{2+} influx across the cellular membrane.[37,38] As expected, the pre-incubation with 1 μM of ionomycin for 1.5 h induced strong green fluorescence in **Fluo-3 AM**-loaded cells, as shown in Fig. 3d3. Compared with that of the green fluorescence in Fig. 3b3, the average fluorescence intensities of cells in Fig. 3d3 increased by 10.03 ($p < 0.01$). Namely, the intracellular Ca^{2+} concentration increased sharply. Moreover, after stimulation with ionomycin, a significant increase was obvious in the red fluorescence intensity of **MB1**-loaded HeLa cells. The average fluorescence intensities of cells in Fig. 3d1 was about 17.64 times ($p < 0.001$) than that in Fig. 3b1. As shown in Fig. S9 (ESI†), the ionomycin itself neither induced the increase in the fluorescence intensity of the **MB1** probe nor interfered with the response to H_2S. Therefore, these results indicated that the H_2S production was related to Ca^{2+} stimulation in the HeLa cells.

Next, we further explored the correlation between the Ca^{2+} and H_2S levels. HeLa cells co-loaded with 5 μM of **MB1** and 1 μM of **Fluo-3 AM** were additionally pre-incubated with 1 μM of

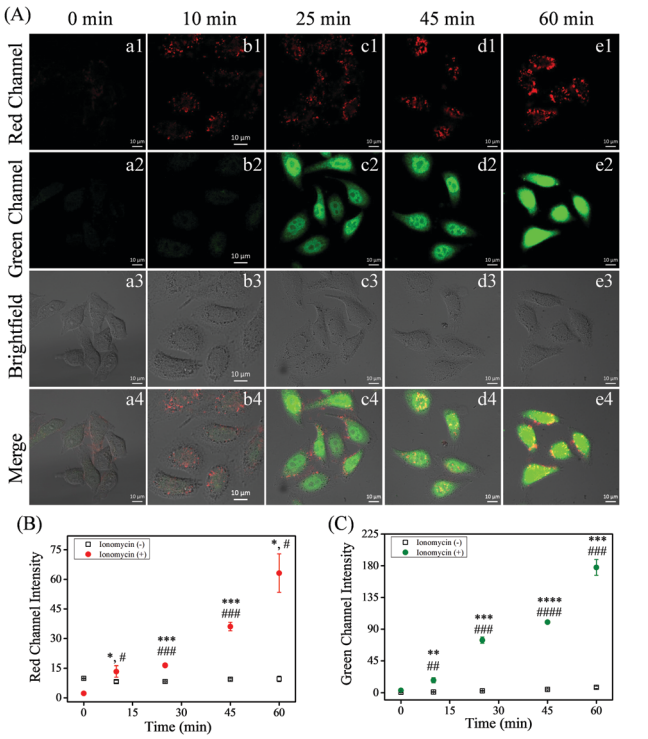

Fig. 4 The CLSM images of **MB1** (5 μM) and **Fluo-3 AM** (1 μM)-loaded HeLa cells. The cells were pre-incubated with ionomycin (1 μM) for 0 min, 10 min, 25 min, 45 min, and 60 min. Red channel, 690 ± 30 nm; λ_{ex} = 633 nm for **MB1**; Green channel, 525 ± 25 nm; λ_{ex} = 488 nm for **Fluo-3 AM**; Scale bar = 10 μm. (B) and (C) Corresponding average fluorescence intensities of cells. Statistical analyses were employed with Student's *t*-test (n = 3). Compared with the 0 min group: $^{*}p < 0.05$, $^{**}p < 0.01$, $^{***}p < 0.001$, and $^{****}p < 0.0001$. Compared with the ionomycin (−) group: $^{\#}p < 0.05$, $^{\#\#}p < 0.01$, $^{\#\#\#}p < 0.001$, $^{\#\#\#\#}p < 0.0001$, and error bars are ±S.D.

ionomycin for different time (0 min, 10 min, 25 min, 45 min, and 60 min) (Fig. 4A). The control group (without ionomycin) is shown in Fig. S10 (ESI†). We found that the fluorescence intensities of the red channel (for **MB1**, Fig. 4a1 to e1) and green channel (for **Fluo-3 AM**, Fig. 4a2 to e2) increased with an increase in the ionomycin incubation time. Compared with the 0 min group, the average fluorescence intensities of the cells incubated with ionomycin for 10 min in red (Fig. 4b1) and green (Fig. 4b2) channels increased 5.86 ($p < 0.05$) and 5.12 ($p < 0.01$) times, respectively. At 10 min, there were statistically significant differences between ionomycin (+) group and ionomycin (−) group (Red channel intensity: Fig. 4B, $p < 0.05$; Green channel intensity: Fig. 4C, $p < 0.01$). Subsequently, with the increase in the ionomycin incubation time, the green channel fluorescence corresponding to **Fluo-3 AM** increased considerably. Moreover, the red fluorescence presented a slow upward trend. At 60 min, compared with the 0 min group, the average fluorescence intensities of the cells in red (Fig. 4e1) and green (Fig. 4e2) channels increased by 24.40 (Fig. 4C, $p < 0.05$) and 50.96 (Fig. 4C, $p < 0.001$) times, respectively. These results indicate that H_2S production was dependent on the Ca^{2+} level in the HeLa cells. Additionally, similar results of Ca^{2+} and H_2S levels were observed by direct incubation of the cells with 200 μM of $CaCl_2$ (Fig. S11, ESI†).

Next, **MB1** was also used to uncover the pathways that result in H_2S production upon Ca^{2+} stimulation of the HeLa cells. For this purpose, the HeLa cells were first pre-incubated with aminooxyacetic acid (AOAA, 100 μM, 3 h), a potent inhibitor of CBS.[39] Then, **MB1** was used to image the change in the cellular H_2S level upon Ca^{2+} (200 μM, 1 h) stimulation. AOAA did not inhibit the increase in the average cellular fluorescence intensity of **MB1** (Fig. 5A). However, the CSE inhibitor, DL-propargylglycine (PAG),[19] absolutely inhibited the turn-on response of **MB1** towards H_2S. Moreover, the average cellular fluorescence intensity decreased from 3.8 to 1.3 ($p < 0.01$, Fig. 5B). This indicated that CSE might contribute to the observed H_2S generation upon Ca^{2+} stimulation.

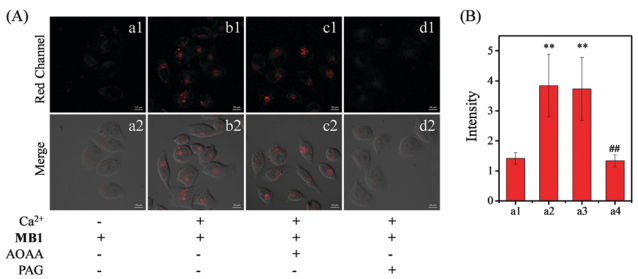

Fig. 5 (A) The CLSM images of the Ca^{2+}-dependent H_2S production pathways. Before imaging, **MB1** (5 μM, 30 min)-loaded HeLa cells were pre-incubated with AOAA or PAG (100 μM, 3 h), and then stimulated with $CaCl_2$ (200 μM, 1 h). Red channel, 690 ± 30 nm, λ_{ex} = 633 nm for **MB1**; Scale bar = 10 μm. (B) Corresponding average fluorescence intensities of cells in (A). Statistical analyses were employed with Student's *t*-test (n = 3). Compared with the a1 group: $^{**}p < 0.01$. Compared with the Ca^{2+}-treated (b1) group: $^{\#\#}p < 0.01$ and error bars are ±S.D.

Conclusion

In summary, we synthesized a highly selective and sensitive fluorescence probe (**MB1**) to visualize the change of H_2S levels in living cells, and to determine the role of intracellular Ca^{2+} in the H_2S homeostasis. Using **MB1**, we imaged the excess H_2S levels in the Ca^{2+}-triggered HeLa cells and studied the dependent effect between them. Furthermore, we provided a potential pathway of the H_2S explosion mediated by Ca^{2+} in living cells, which provides new insights into the complex signal transduction in living cells.

Conflicts of interest

There are no conflicts to declare.

Acknowledgements

We thank the National Natural Science Foundation of China (No. 21705102, 21775096), the Shanxi Province Science Foundation for Youths (No. 201701D221061) Shanxi Province Foundation for Returness (No. 2017-026), One hundred people plan of Shanxi Province, Shanxi Province ''1331 Project'' Key Innovation Team Construction Plan Cultivation Team (2018-CT-1), Shanxi Province Foundation for Returness (2017-026), Shanxi Collaborative Innovation Center of High Value-added Utilization of Coal-related Wastes, 2018 Xiangyuan County Solid Waste Comprehensive Utilization Science and Technology Project 2018XYSDJS-05, China Institute for Radiation Production and Scientific Instrument Center of Shanxi University (201512). Ying Wen also thanks Dr Peng Wei and Professor Tao Yifrom Fudan University for the gift of **FDOCl-2**.

Notes and references

1 M. R. Filipovic, J. Zivanovic, B. Alvarez and R. Banerjee, *Chem. Rev.*, 2018, **118**, 1253–1337.
2 R. Wang, *Trends Biochem. Sci.*, 2014, **39**, 227–232.
3 H. Kimura, *Antioxid. Redox Signaling*, 2015, **22**, 362–376.
4 C. Coletta, A. Papapetropoulos, K. Erdelyi, G. Olah, K. Modis, P. Panopoulos, A. Asimakopoulou, D. Gero, I. Sharina, E. Martin and C. Szabo, *Proc. Natl. Acad. Sci. U. S. A.*, 2012, **109**, 9161–9166.
5 R. Wang, *Physiol. Rev.*, 2012, **92**, 791–896.
6 T. V. Mishanina, M. Libiad and R. Banerjee, *Nat. Chem. Biol.*, 2015, **11**, 457–464.
7 S. Fiorucci, E. Distrutti, G. Cirino and J. L. Wallace, *Gastroenterology*, 2006, **131**, 259–271.
8 P. K. Kamat, P. Kyles, A. Kalani and N. Tyagi, *Mol. Neurobiol.*, 2016, **53**, 2451–2467.
9 S. K. Jain, R. Bull, J. L. Rains, P. F. Bass, S. N. Levine, S. Reddy, R. McVie and J. A. Bocchini, *Antioxid. Redox Signaling*, 2010, **12**, 1333–1337.
10 P. Kamoun, M. C. Belardinelli, A. Chabli, K. Lallouchi and B. Chadefaux-Vekemans, *Am. J. Med. Genet., Part A*, 2003, **116**, 310–311.

11 G. Meng, Y. Ma, L. Xie, A. Ferro and Y. Ji, *Br. J. Pharmacol.*, 2015, **172**, 5501–5511.
12 N. Shibuya, S. Koike, M. Tanaka, M. Ishigami-Yuasa, Y. Kimura, Y. Ogasawara, K. Fukui, N. Nagahara and H. Kimura, *Nat. Commun.*, 2013, **4**, 1366.
13 Y. Mikami, N. Shibuya, Y. Kimura, N. Nagahara, M. Yamada and H. Kimura, *J. Biol. Chem.*, 2011, **286**, 39379–39386.
14 G. Yang, L. Wu, B. Jiang, W. Yang, J. Qi, K. Cao, Q. Meng, A. K. Mustafa, W. Mu, S. Zhang, S. H. Snyder and R. Wang, *Science*, 2008, **322**, 587–590.
15 Y. Mikami, N. Shibuya, Y. Ogasawara and H. Kimura, *Biochem. Biophys. Res. Commun.*, 2013, **431**, 131–135.
16 V. S. Lin, W. Chen, M. Xian and C. J. Chang, *Chem. Soc. Rev.*, 2015, **44**, 4596–4618.
17 Y. Chen, C. Zhu, Z. Yang, J. Chen, Y. He, Y. Jiao, W. He, L. Qiu, J. Cen and Z. Guo, *Angew. Chem., Int. Ed.*, 2013, **52**, 1688–1691.
18 S. K. Bae, C. H. Heo, D. J. Choi, D. Sen, E. H. Joe, B. R. Cho and H. M. Kim, *J. Am. Chem. Soc.*, 2013, **135**, 9915–9923.
19 V. S. Lin, A. R. Lippert and C. J. Chang, *Proc. Natl. Acad. Sci. U. S. A.*, 2013, **110**, 7131–7135.
20 Y. Wen, K. Liu, H. Yang, Y. Li, H. Lan, Y. Liu, X. Zhang and T. Yi, *Anal. Chem.*, 2014, **86**, 9970–9976.
21 Y. Wen, W. Zhang, T. Liu, F. Huo and C. Yin, *Anal. Chem.*, 2017, **89**, 11869–11874.
22 J. Kang, F. J. Huo, P. Ning, X. M. Meng, J. B. Chao and C. X. Yin, *Sens. Actuators, B*, 2017, **250**, 342–350.
23 R. Zhang, J. Zhao, G. Han, Z. Liu, C. Liu, C. Zhang, B. Liu, C. Jiang, R. Liu, T. Zhao, M. Y. Han and Z. Zhang, *J. Am. Chem. Soc.*, 2016, **138**, 3769–3778.
24 P. Ou, R. Zhang, Z. Liu, X. Tian, G. Han, B. Liu, Z. Hu and Z. Zhang, *Angew. Chem., Int. Ed.*, 2019, **58**, 2261–2265.
25 L. Tang, M. Tian, H. Chen, X. Yan, K. Zhong and Y. Bian, *Dyes Pigm.*, 2018, **158**, 482–489.
26 M. Xu, S. P. Kelley and T. E. Glass, *Angew. Chem., Int. Ed.*, 2018, **57**, 12741–12744.
27 L. Zhang, X. A. Liu, K. D. Gillis and T. E. Glass, *Angew. Chem., Int. Ed.*, 2019, **58**, 7611–7614.
28 P. Wei, W. Yuan, F. Xue, W. Zhou, R. Li, D. Zhang and T. Yi, *Chem. Sci.*, 2018, **9**, 495–501.
29 J. Bae, L. E. McNamara, M. A. Nael, F. Mahdi, R. J. Doerksen, G. L. Bidwell, N. I. Hammer and S. Jo, *Chem. Commun.*, 2015, **51**, 12787–12790.
30 B. Chen, P. Wang, Q. Jin and X. Tang, *Org. Biomol. Chem.*, 2014, **12**, 5629–5633.
31 D. Aydin Tekdas, R. Garifullin, B. Senturk, Y. Zorlu, U. Gundogdu, E. Atalar, A. B. Tekinay, A. A. Chernonosov, Y. Yerli, F. Dumoulin, M. O. Guler, V. Ahsen and A. G. Gurek, *Photochem. Photobiol.*, 2014, **90**, 1376–1386.
32 A. Ogunsipe, J.-Y. Chen and T. Nyokong, *New J. Chem.*, 2004, **28**, 822–827.
33 R. G. Lebel and D. A. I. Goring, *J. Chem. Eng. Data*, 1962, **7**, 100–101.
34 M. Kim, Y. H. Seo, Y. Kim, J. Heo, W. D. Jang, S. J. Sim and S. Kim, *Chem. Commun.*, 2017, **53**, 2275–2278.
35 F. Yu, X. Han and L. Chen, *Chem. Commun.*, 2014, **50**, 12234–12249.
36 X. Wang, J. Sun, W. H. Zhang, X. X. Ma, J. Z. Lv and B. Tang, *Chem. Sci.*, 2013, **4**, 2551–2556.
37 C. Yang, Y. Qin, D. Jiang and H. Y. Chen, *ACS Appl. Mater. Interfaces*, 2016, **8**, 19892–19898.
38 S. Zhou, X. Peng, H. Xu, Y. Qin, D. Jiang, J. Qu and H. Y. Chen, *Anal. Chem.*, 2018, **90**, 7982–7988.
39 C. Chao and J. R. Zatarain, *Mol. Med.*, 2016, **22**, 361–379.

